Pergamon

Journal of Structural Geology, Vol. 20, No. 12, pp. 1733 to 1746, 1998

0191-8141/98/$ - see front matter

PII: S0191-8141(98)00087-X

Fluid inclusion evidence for progressive folding during decompression in metasediments of the Voltri Group (Western Alps, Italy)

LAURA CRISPINI

Dipartimento di Scienze della Terra, Corso Europa 26, 16132 Genova, Italy, E-mail: capponi@dister.unige.it

and

MARIA-LUCE FRE'ZZOTTI

Dipartimento di Scienze della Terra, Via delle Cerchia 3, 53100 Siena, Italy

(*Received* 9 *February* 1998; *accepted in revised form* 27 *July* 1998)

Abstract—Quartz veins syntectonic to distinct folding events in metasediments from the Voltri Group (Ligurian Alps) were studied in order to compare fluid and structural evolution. Studied veins (VS1, VS2, VS3) pertain to three distinct generations of folds (F_1, F_2, F_3) that formed during the retrograde metamorphic evolution. Two types of fluids characterize the different generations of veins and are represented essentially by aqueo-carbonic mixtures of moderate salinity with decreasing densities (1.01–0.41 g/cm^3). The chemical evolution is characterised by a progressive decrease of H_2O, from early fluids associated with opening of VS1 and VS2 ($XCO_2 \approx 0.08$) to fluids related to VS3 formation ($XCO_2 \approx 0.3$). The close match between the fluids in VS1 and VS2 suggests that the development of two superimposed systems of folds (F_1 and F_2 folds) occurs under very similar P–T conditions, during a progressive and continuous deformational event at glaucophanic and/or barroisitic metamorphic grade. A different evolution is outlined for the formation of VS3 during low greenschist grade. Successive isochores allow us to define a retrograde decompression path for the Voltri Group. Present results indicate that fluid inclusions are powerful markers to constrain the P–T–t conditions of different folding events. © 1998 Elsevier Science Ltd. All rights reserved

INTRODUCTION

Fluid inclusions in metamorphic rocks may give useful indications and constraints on the composition and trapping conditions of the fluid phases present during the tectono-metamorphic evolution of a metamorphic belt. In the last two decades, the quality of fluid inclusion analysis has been greatly improved mainly because of a better understanding of physico-chemical properties of fluid systems combined with the development of *in situ* analyses (Hollister and Crawford, 1981; Roedder, 1984; Shepherd *et al*., 1985; Touret, 1987; De Vivo and Frezzotti, 1994). In addition recent experimental studies (Sterner and Bodnar, 1989; Bodnar *et al*., 1989; Bakker and Jansen, 1990, 1991, 1994; Sterner *et al*., 1995; Vityk and Bodnar, 1995a,b) have provided clues to predict the fluid inclusion evolution with respect to the overall rock exhumation path (e.g. isobaric cooling vs decompression); they have shown how changes in composition and density may be the rule more than the exception. However, if carefully analysed, fluid inclusions may provide very useful information on P–T–t path of metamorphic rocks and on the overall fluid–rock interaction history. Boullier *et al*. (1991), Hodgkins and Stewart (1994) and Mullis (1996) have investigated the link between fluids and tectonic evolution.

In the present work we sampled three sets of syntectonic quartz and carbonate veins in the metasediments of the Voltri Massif (northwest Alps; Chiesa *et al*., 1975). These veins show clear field chronological relationships and are related to folding structures. The purpose of the present study is to analyse fluids with respect to the structural evolution in order to assign the structures observed in outcrop to a precise tectono-metamorphic event when diagnostic mineralogical assemblages are absent. We concentrate on:

1. the synmetamorphic structural evolution of the Voltri Group metasediments, with respect to the orogenic phases;
2. the chemical composition of fluids and their evolution during the late stages of the structural and metamorphic evolution of the metasediments;
3. the P–T–X conditions and pressure regimes active during fluid trapping and the pressure–temperature conditions during which veins and folds evolved.

GEOLOGICAL SETTING

The Voltri Group is a meta-ophiolitic massif including metasediments at the southeast margin of the Western Alps (Fig. 1). It consists mainly of serpentinites with metagabbros and eclogitic bodies, metasediments (*Schistes Lustrés*, Auct.) with metabasites, and meta-lherzolites with minor pyroxenite and dunite bodies (Chiesa *et al*., 1975; Capponi, 1991). The entire massif suffered Alpine subduction and metamorphism

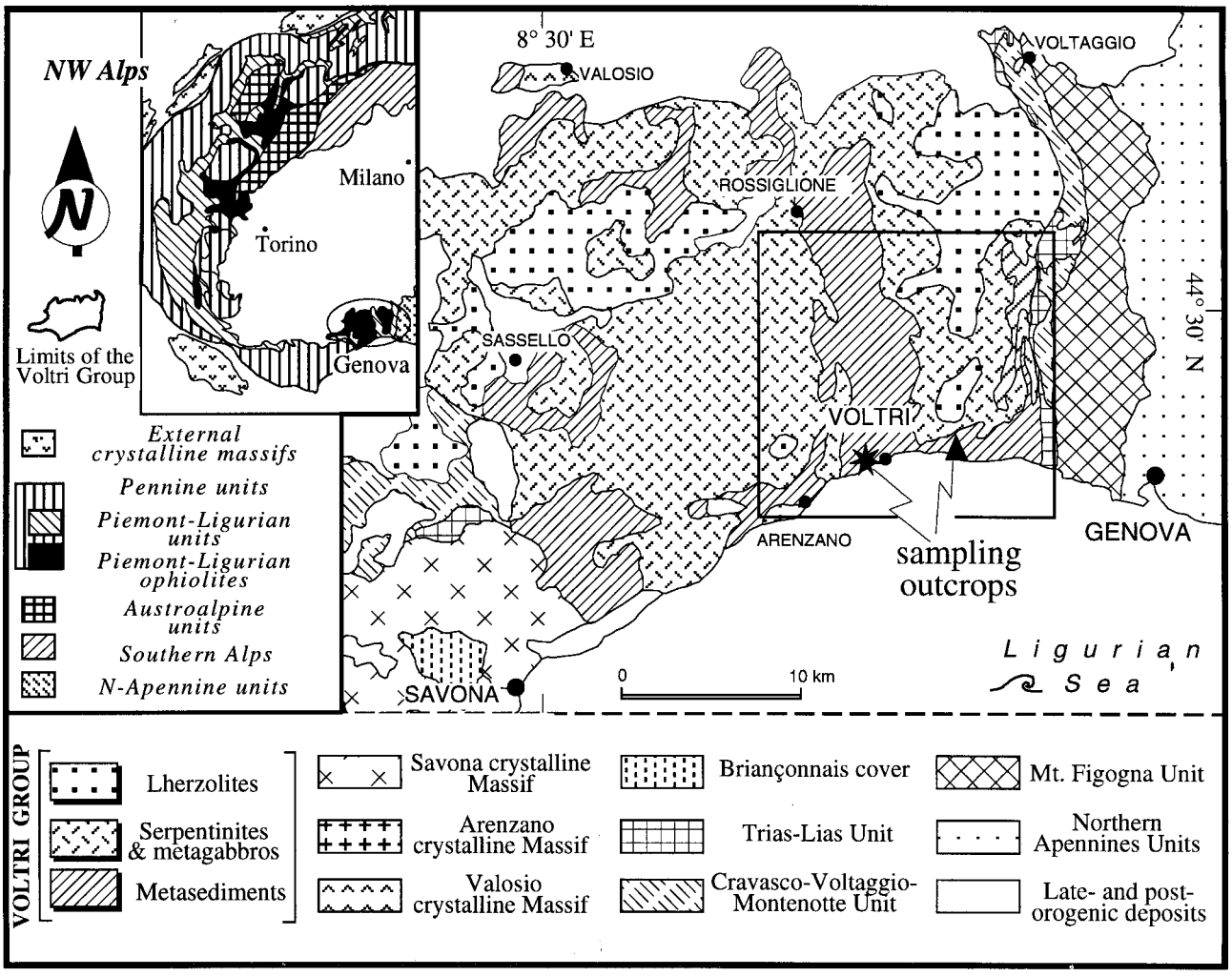

Fig. 1. Structural sketch map of the Voltri Group and surrounding units (redrawn from Crispini and Capponi, 1997). Inset indicates the study area.

(Cabella *et al.*, 1994 and references therein). The metamorphic evolution of the Voltri Group (Fig. 2) has been extensively studied in the mafic and ultramafic rocks which preserve relics of mineralogical associations of the different metamorphic stages (Cabella *et al.*, 1994 and references therein): eclogite facies with $P > 20$ kbar and $T > 500°C$ to blueschists facies $P \geq 10$ kbar and $T > 450°C$ (Cortesogno *et al.*, 1977; Hoogerduijn Strating, 1991; Cabella *et al.*, 1994; Messiga *et al.*, 1995), followed by decompression down to greenschist facies conditions ($P = 4$ kbar and $T = 350°C$). This metamorphic evolution is less apparent in the metasediments, mainly because of the rarity of diagnostic mineralogical assemblages.

Deformation and metamorphism

The overall deformation of the metasediments of the Voltri Group is characterized by a complex history developed in a rotational shear regime, commonly with a non-coaxial component of deformation (Hoogerduijn Strating, 1991; Crispini, 1996; Crispini and Capponi, 1997). The folding evolution can be summarized by five superimposed folding events (pre-F_1 to F_4), developed during decompression after the high-pressure stages of the tectono-metamorphic evolution. In general, the structures related to the high-pressure metamorphic stages (pre-F_1 structures) are preserved only as relics in certain domains (Capponi, 1991; Crispini, 1996), while the main folding events (F_1–F_2–F_3) are coeval with the retrograde metamorphic evolution down to greenschist facies metamorphism. F_1 and F_2 folds are tight to isoclinal in shape with schistosity parallel to the axial plane and sometimes with complete transposition of the hinge zones. Sheath folds also occur (Crispini and Capponi, 1997).

F_1 and F_2 folding structures are overprinted by typical mylonitic features such as asymmetric extensional shear bands (Hanmer and Passchier, 1991) or extensional crenulation cleavage (Platt and Vissers, 1980) and asymmetric foliation boudinage, testifying to a deformational regime with maximum extension nearly parallel to the foliation surfaces. Both F_1–F_2 folds and the mylonitic structures can be intepreted as resulting from a variation in the relative orientation of the maximum longitudinal strain and rock anisotropies

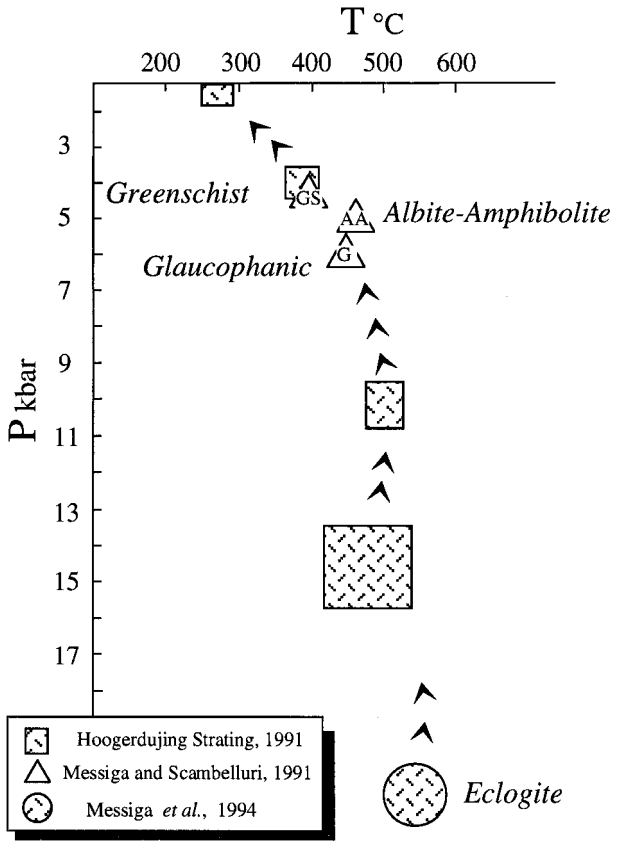

Fig. 2. *P–T* diagram summarizing the thermobarometric conditions inferred for mafic lithotypes of the Voltri massif; data and trajectories redrawn from Hoogerduijn Strating (1991), Messiga and Scambelluri (1991) and Messiga *et al.* (1995).

during a continuous and progressive deformation event, developed under decreasing pressure conditions.

The F_3 folding episode represents the last significant synmetamorphic deformation event and is characterized by parallel folds, gentle to open in shape and locally associated with a rough spaced cleavage but rarely with a schistosity. F_4 folds are linked to regional thrust tectonic and are characterized by wavelengths up to 1 kilometre. F_4 folds are rarely accompanied by metamorphic recrystallization, and locally zeolite facies minerals have developed.

Sample locations

From a structural point of view, the southeast sector of the Voltri Group (square in Fig. 1) represents the hinge-zone of a kilometre-scale fold (F_2) involving ultramafites, mafic lithotypes and metasediments (Capponi, 1991; Crispini, 1996). This hinge-zone is characterized by common folds with 'M' asymmetry and by high angles between F_2 related schistosity (S_2) and the Main Foliation 1 (MF1) composed of the lithologic banding and the F_1 related schistosity, different from what is commonly observed in other sectors of the Voltri Group. MF1 shows a general ENE–WSW trend and S_2 generally dips towards the east with a north–south trend (Fig. 3).

The paucity of outcrops and the heterogeneous distribution of deformations over the outcrops, combined with the lack of diagnostic metamorphic assemblages, often preclude the comprehension of the relationships between deformation and metamorphism on a large scale. Two sampling sites have been chosen in outcrops which are among the most representative of the south eastern sector of the Voltri Group (Fig. 1). The sampling sites (Fig. 1) have structural features in common and are characterized by a system of similar F_2 folds with axial plane surfaces trending north–south and dipping to the east (Fig. 4). In the metapelitic layers axial planes are represented by a pervasive schistosity along which white micas and epidote recrystallise. Lithologic banding is affected by tectonic repetition caused by isoclinal F_1 folds (Capponi, 1991; Crispini, 1996). F_1 structures are represented by intrafolial folds. F_1 and F_2 axial planar surfaces are gently refolded by F_3 folds that show a decametric to kilo-

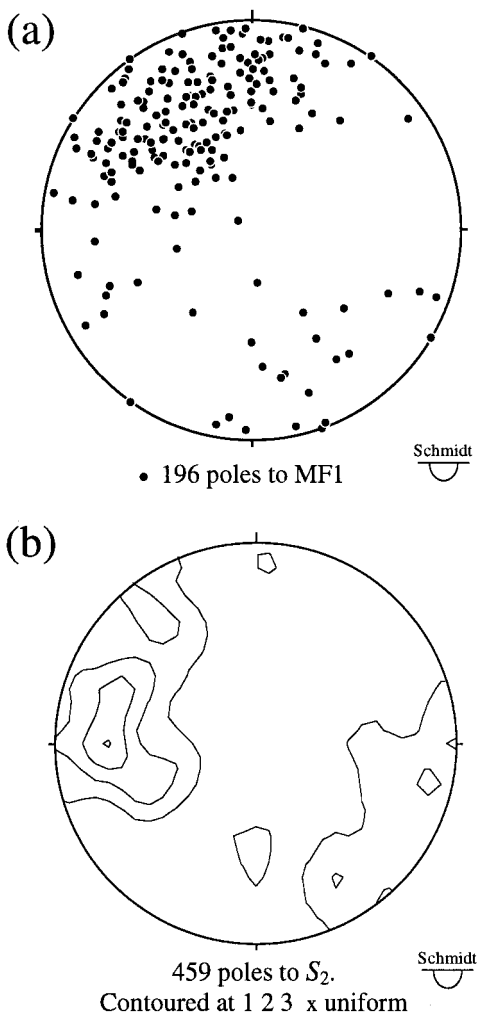

Fig. 3. Stereoplot (lower hemisphere) of the main foliation 1 (a) and density plot of the F_2 related schistosity (b) in the metasediments of the southeast sector of the Voltri Group. The diagrams outline the main characteristics of this sector of the massif: MF1 shows a general ENE–WSW attitude and S_2 shows maxima for N–S direction and dip towards the east.

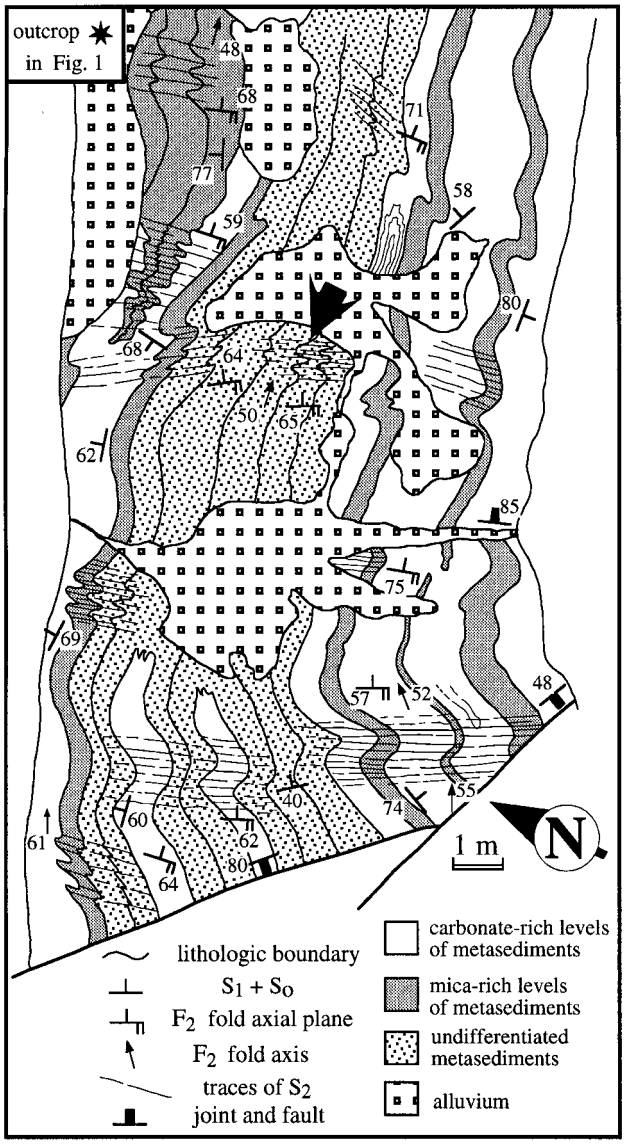

Fig. 4. Schematic geologic map of a sampled outcrop (* in Fig. 1) representative of the main structural setting of the south-eastern sector of the Voltri Group. The arrow shows the locus of Fig. 5.

metric wavelength. Two boudinage events affect F_2 folds in metasediments: (a) symmetric boudinage characterized by regular necks every 10–20 cm with carbonate infilling; (b) boudinage at a larger scale that affects marble layers with necks filled by chlorite, albite and carbonates. The structures described above are cut by distinct systems of veins, in some cases with clear geometric intersection relationships described below.

Petrography

The metasediments consist of prevalent centimetric to decimetric light-grey carbonate layers alternating with black metapelitic layers; these are intersected by numerous quartz-carbonatic veins. In the metapelitic layers, the mineral association is characterized by ubiquitous white mica (phengite, muscovite) and chlorite with inclusions of graphite. In few cases chloritoid has been observed in association with phengite and chlorites. Graphite is present as small (5 μm) flakes with a preferred orientation defining the main foliation within metapelitic levels, and as rounded pseudomorphic microstructures overgrowing garnet and/or chloritoid. Light coloured layers are usually composed of carbonates (70–80%), quartz (20–10%), chlorites and feldspars (up to 10%); a few decimetre-thick layers contain up to 90% of carbonates. White micas are in stable association with Fe-chloritoid, chlorites $\pm$ quartz.

In chloritoid rich levels, representative microstructures indicate that different mineral associations are linked to F_1 and F_2 structures, but no diagnostic mineral assemblages have been observed. Kinked white mica 1 (first generation of white mica), occurs in the hinge zones of F_2 folds; these are phengites with Si^{4+} value between 3.49 and 3.5 a.p.f.u. and are stable with Fe-chloritoid 1 + chlorite $\pm$ quartz (Crispini, 1996). White mica 2 grows along S_2 (F_2 related schistosity) and is a phengite with Si^{4+} value between 3.37 and 3.48 a.p.f.u. stable with Fe-chloritoid 2 + chlorite. White mica 3 lies along post-F_1–F_2 shear bands and is a muscovite stable with Fe-chloritoid 3. No compositional differences have been detected among the three generations of Fe-chloritoid.

VEIN SYSTEMS

Macrostructure

Three sets of veins have been sampled (four samples for each set) for fluid inclusion analysis. These have been distinguished by their mutual crosscutting relationships and their chronological relationships with other structures (folds and shear bands). Field relationships between veins and folds are illustrated in Figs 5 and 6. The veins have been distinguished as follows:

Vein set 1 (VS1)—pretectonic to F_2 folds and clearly deformed by this phase.

Vein set 2 (VS2)—syntectonic to F_2 folds.

Vein set 3 (VS3)—post-F_2, syntectonic to F_3 folds.

VS1 attitudes are scattered along a great circle (Fig. 7) and show a partial coincidence with VS2. VS1 are parallel to S_2 in tight F_2 folds. Veins of set 2 are partially reoriented by the superposed F_3 open folds.

Vein set 1—Veins of the first set have a thickness between 5 and 10 cm, probably accommodating an early bedding-normal extension. VS1 are composed mainly of quartz; sometimes they show reactivation with secondary crystallization of carbonates. Vein walls are nearly parallel to lithological boundaries. Locally veins are folded with lithological boundaries. In the hinge zone of F_2 folds the vein walls are transposed into parallism with the F_2 axial plane (Fig. 5). In these transposition sites VS1 shows a pervasive in-

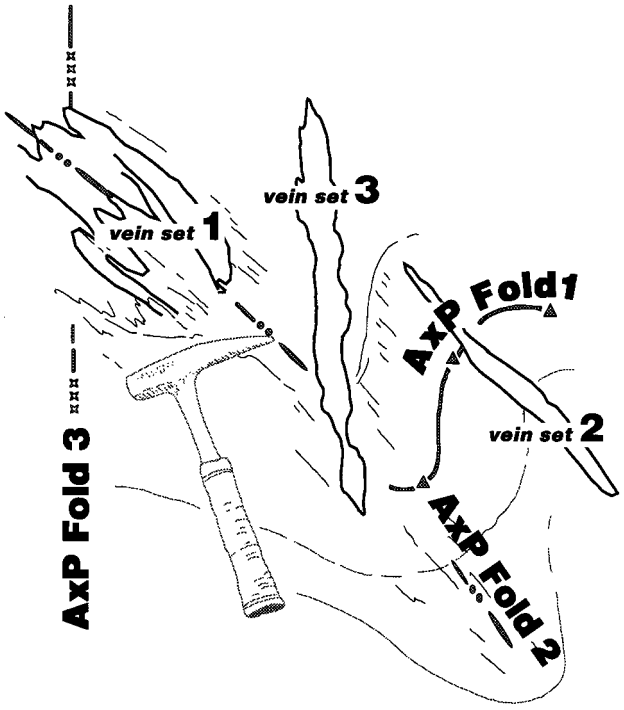

Fig. 5. Schematic field chronological relationships between folds and veins from the outcrop in Fig. 4. Veins of set 1 are pretectonic to F_2 folds and folded; veins of set 2 are syntectonic to F_2 folds; veins of set 3 cut F_2 folds and are syntectonic to F_3 folds (only axial plane of F_3 is shown because of the large scale of these folds). (AxP = Axial Plane of the fold.) Redrawn from a photograph; hammer for scale.

ternal deformation with the development of cleavage and microcataclasis. Other VS1 veins, which are occasionally boudinaged, show no internal deformation inside the boudins or along the limbs of F_2 folds. These undeformed sites have been selected for fluid inclusion study.

Vein set 2—In the second system, veins are 2–3 cm in thickness, in few cases up to 5 cm wide, and usually have parallel and straight margins. They commonly consist of both quartz and calcite. Crystals grow normal to the vein walls. In composite veins, quartz grows from the vein walls as crystals or 1 cm-long fibres while calcite lies in the central part of the vein. Cracking and filling of VS2 veins can be considered syntectonic to F_2 folds; VS2 walls are nearly parallel to axial plane surfaces of F_2 folds (Fig. 7) and commonly cut the lithologic banding and intrafoliar F_1 folds (Fig. 5). VS2 veins are neither pervasively deformed nor transposed, and are less deformed than VS1 veins.

Vein set 3—The third system of veins is represented by stretched fibre veins (Ramsay and Huber, 1987) consisting only of quartz. They are at most 2.5 cm in thickness and are narrower than VS1 and VS2. VS3 veins cut all the main structures (Fig. 5). They developed with the same attitude as the cleavage of F_3 folds and show a syn-cleavage origin.

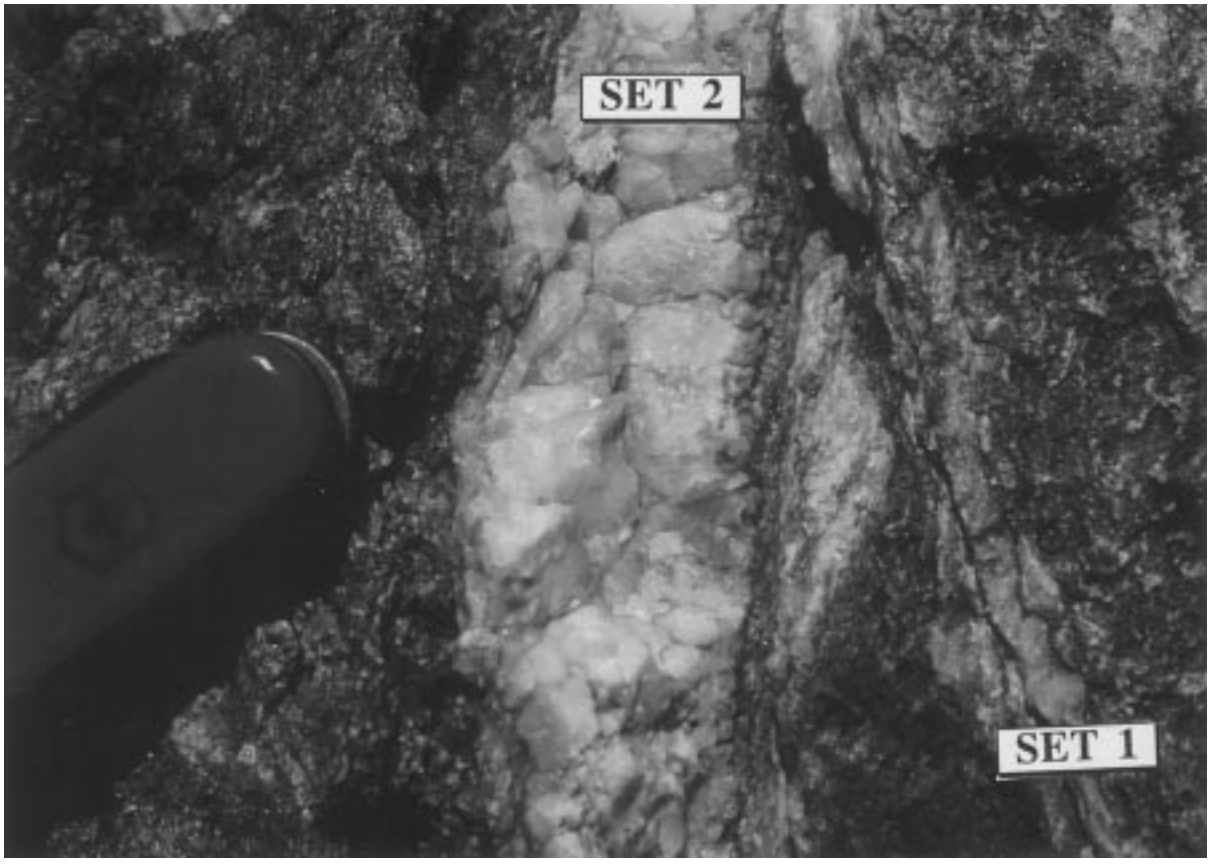

Fig. 6. Quartz vein of vein set 2 crosscutting a vein of set 1 (the vein on the right); S_2 trace is vertical. Knife for scale.

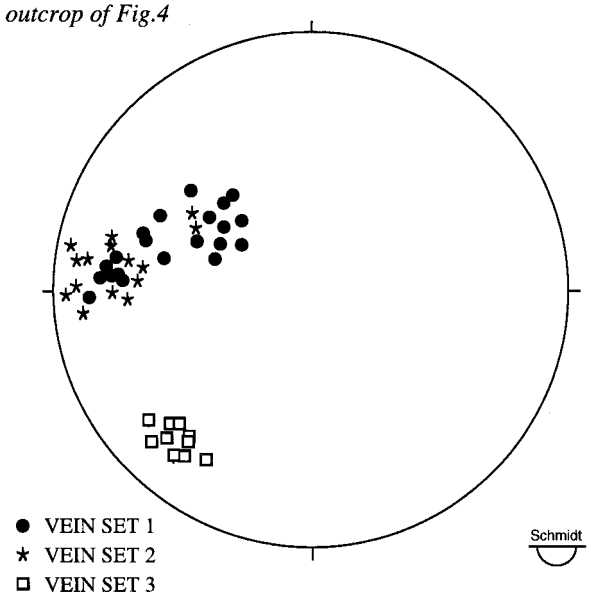

Fig. 7. Stereoplot (lower hemisphere) of poles to sampled veins. Veins of set 2 are partially reoriented by the superposed F_3 open folds. Veins of set 1 have been deformed into parallel with S_2 (see Fig. 2).

Microstructure

Since microstructural features in VS1 and VS2 are similar, these two vein sets will be discussed together. In both sets of veins, subhedral quartz grains, 5–10 mm in diameter, grow normal to vein walls. No macroscopic deformation is evident in quartz. Conversely, a small-scale strain partitioning is recognized under the microscope; it gives rise to a heterogeneous distribution of strained and undeformed sites. In the strained sites, quartz grains show undulatory extinction, deformation lamellae and deformation bands, as well as subgrain formation. A strong quartz crystallographic preferred orientation can be detected with the gypsum plate at sites where quartz grains have interlobate shapes with irregular grain boundaries, grain-boundary migration seems to be prevalent. In other microdomains, newly formed quartz grains (100×100 μm) follow the crystallographic orientation of the host grain: in this last case dynamic recrystallization occurs as subgrain rotation. The transition between grain boundary migration and grain rotation in quartz deformation mechanisms is present in all samples.

Some preserved or recrystallized grains lack internal deformations. Generally very late recrystallization processes form new sub-equant grains (0.2–0.5 mm) with a polygonal texture.

In VS2 syntaxial composite veins, carbonates fill the central part of the vein and/or crystallize in pull-apart microfractures between quartz fibers. Carbonate grains show more intense deformation features than neighbouring quartz, with folded twin lamellae of the type III–IV of Burkhard (1993).

Vein set 3 (VS3)—Quartz shows a granoblastic polygonal texture with no relics of crystallographic preferred orientation. The main grain size is 30–40 μm. No ductile deformation has been observed, and quartz grains are pervaded by late systems of microfractures.

P–T conditions and veining events

The temperature limits of veining events can be inferred from the P–T–X path depicted in Fig. 2, based on diagnostic metamorphic mineral assemblages in the mafic lithotypes (Cabella *et al.*, 1994 and references therein), since they underwent the same P–T evolution as the metasediments. For VS1 and VS2, a range of temperatures between 400 and 450°C can be considered reliable and is consistent with the observed transition between grain boundary migration–grain rotation in quartz deformation mechanisms that occurs at about 400–420°C (Werling, 1992).

An additional pressure calculation for the folding events has been obtained from the equilibrium curves of Velde (1967) on phengites of the previously described mineralogical associations in the metasediments. We can estimate a minimum value (as K-feldspar is absent) of about 7–8 kbar for F_1 folding and of about 6 kbar for F_2 event (Fig. 8a). Although this geobarometer is not universally accepted, Velde (1967) curves seem more suitable to the low temperatures in this study, than the experimental data of Massonne and Schreyer (1987). Calculated P–T conditions fit the glaucophanic and/or barroisitic stage estimated by Cimmino and Messiga (1979) and Messiga and Scambelluri (1991) for mafic lithotypes (Fig. 2).

FLUID INCLUSIONS

Analytical techniques

Twelve vein samples were collected in the two investigated localities shown in Fig. 1; three thin sections were prepared per oriented sample for microstructural investigation: two thin sections were cut normal to the vein wall and parallel to dip-direction to cover the entire thickness of a single vein, the third one was cut normal to the vein wall and to the other thin sections. Fluid inclusion studies were made on three oriented doubly-polished plates approximately 100 μm thick plates, representative of each vein set.

Microthermometry was performed on about 150 fluid inclusions with the use of a Chaix-Meca heating–freezing stage (Poty *et al.*, 1976) at the Department of Earth Sciences in Siena. Calibration was carried out using natural and synthetic standards. An ice bath was used to calibrate for 0°C. The low temperature calibration included measurements of the CO_2 triple point in natural $H_2O + CO_2$ inclusions, and ethylacetate (–83°C). At high temperatures, synthetic Merk sub-

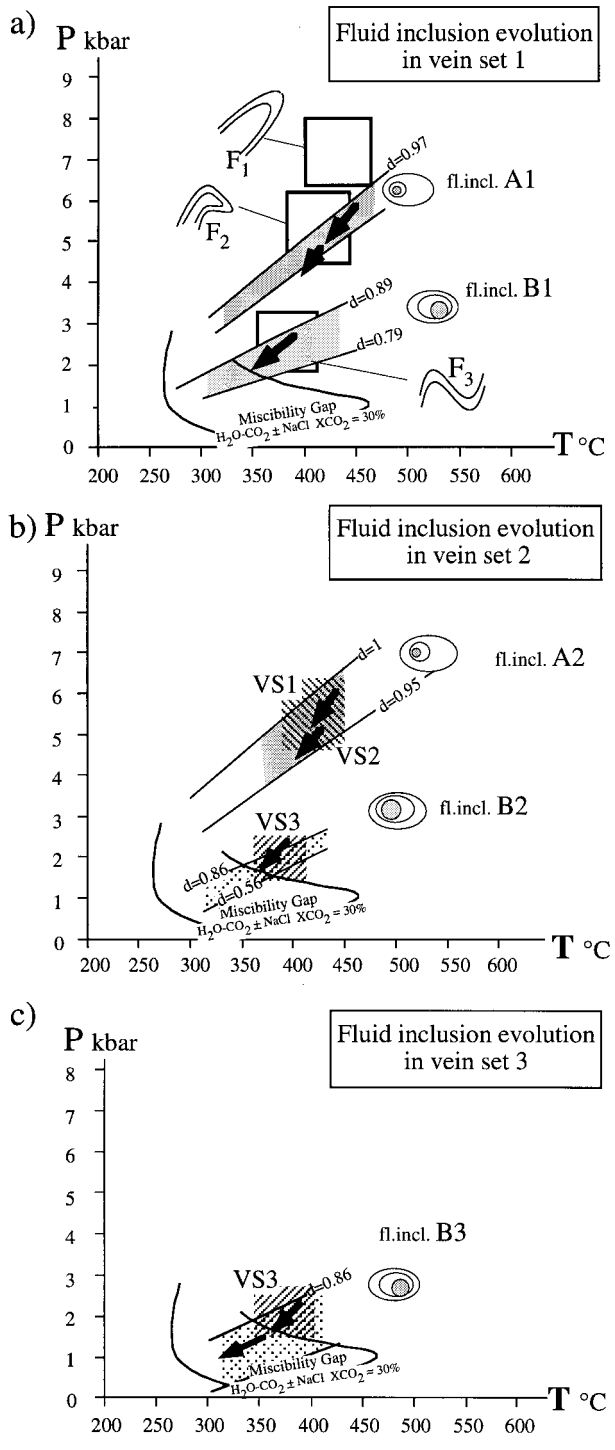

Fig. 8. Pressure–temperature diagram showing the calculated isochores for the least- and most-dense (shaded areas) fluid for type A1, A2, and B1, B2, B3 fluid inclusions in the different vein sets. (a) Vein set 1. White boxes indicate *P–T* conditions inferred for the folding events from petrographic analysis in the metasediments. (b) Vein set 2. (c) Vein set 3. Dashed boxes indicate *P–T* conditions inferred for the veining events. A possible uplift path for the Voltri metasediments consistent with petrologic and fluid inclusions data is shown by arrows. The miscibility gaps for the H_2O–CO_2 ($X_{CO_2} = 30$ mol.%) and H_2O–CO_2–NaCl ($X_{CO_2} = 30$ mol.%; $X_{NaCl} = 5$ wt%) systems (Gehrig *et al.*, 1979 and Gehrig, 1980) are reported.

stances of known melting point were used for calibration. The reproducibility of these melting point measurements is ±0.2°C at a heating rate of 0.1°C/min. Data collected from fluid inclusions include final melting (Tm) of the CO_2-rich phase and the clathrate phase, and homogenization (Th) of the CO_2-rich phases.

Volumetric proportions of carbonic and water-rich phases in the inclusions ($F = V_{H_2O}/V_{H_2O} + V_{CO_2}$) were estimated optically in regular shaped inclusions using the reference charts from Shepherd *et al.* (1985).

Mole fractions of CO_2 and CH_4 were determined by Raman microspectroscopy in individual inclusions with a DILOR *X–Y* multichannel Raman spectrometer, at the CREGU in Nancy.

Composition, density and isochores of fluid inclusions were calculated using the MacFlincor (Brown and Hagemann, 1994) program, using equations of state by Bowers and Helgeson (1983) for $CO_2 + H_2O$ inclusions, and by Brown and Lamb (1989) and Zhang and Frantz (1987) for water dominated inclusion. Clathrate stability conditions have been verified with the software program Q2 (Bakker, 1995, 1997). f_{O_2} conditions for the fluid phase in inclusions were calculated using Flevol software (Bakker, 1992).

Types of fluid inclusions

Fluid inclusions were examined in quartz crystals from the different veins collected in the two localities reported in Fig. 1. Different types of aqueo-carbonic fluid inclusions have been observed inside quartz in each vein set. The relative chronology between fluid trapping, quartz growth or deformation has been studied with respect to the geometric features of micro- to macro-structures of the host rocks. In all veins, three-phase mixed CO_2–H_2O inclusions ($V_{CO_2} + L_{CO_2} + L_{H_2O}$) with different CO_2/H_2O volumetric ratios dominate. Rare two-phase CO_2 inclusions ($L + V$) and two-phase H_2O inclusions ($L + V$) are also present. No daughter minerals have been observed. Solid inclusions represented by carbonates, chlorites, and graphite, are occasionally present along microfractures.

Quartz microstructures and fluid inclusion distribution allow recognition of three main types of fluid inclusions with variable CO_2–H_2O percentage (Fig. 9):

Type A inclusions are water dominated mixed CO_2–H_2O inclusions. These have mature ellipsoidal shapes and are the largest inclusions present (> 5–20 μm). At room temperature they usually contain three-phases: vapour and liquid CO_2 surrounded by liquid H_2O (Fig. 9); the volume percentage of the outer aqueous phase is in the range of 70–80%. In some cases, highly irregular star-shaped inclusions which exhibit textures with decrepitation features under condition of external underpressure are observed (Vityk and Bodnar, 1995a,b). In these last ones, H_2O volume fractions are variable but do not exceed 50% of the whole inclusion volume, indicating that water-loss occurred during re-equilibration.

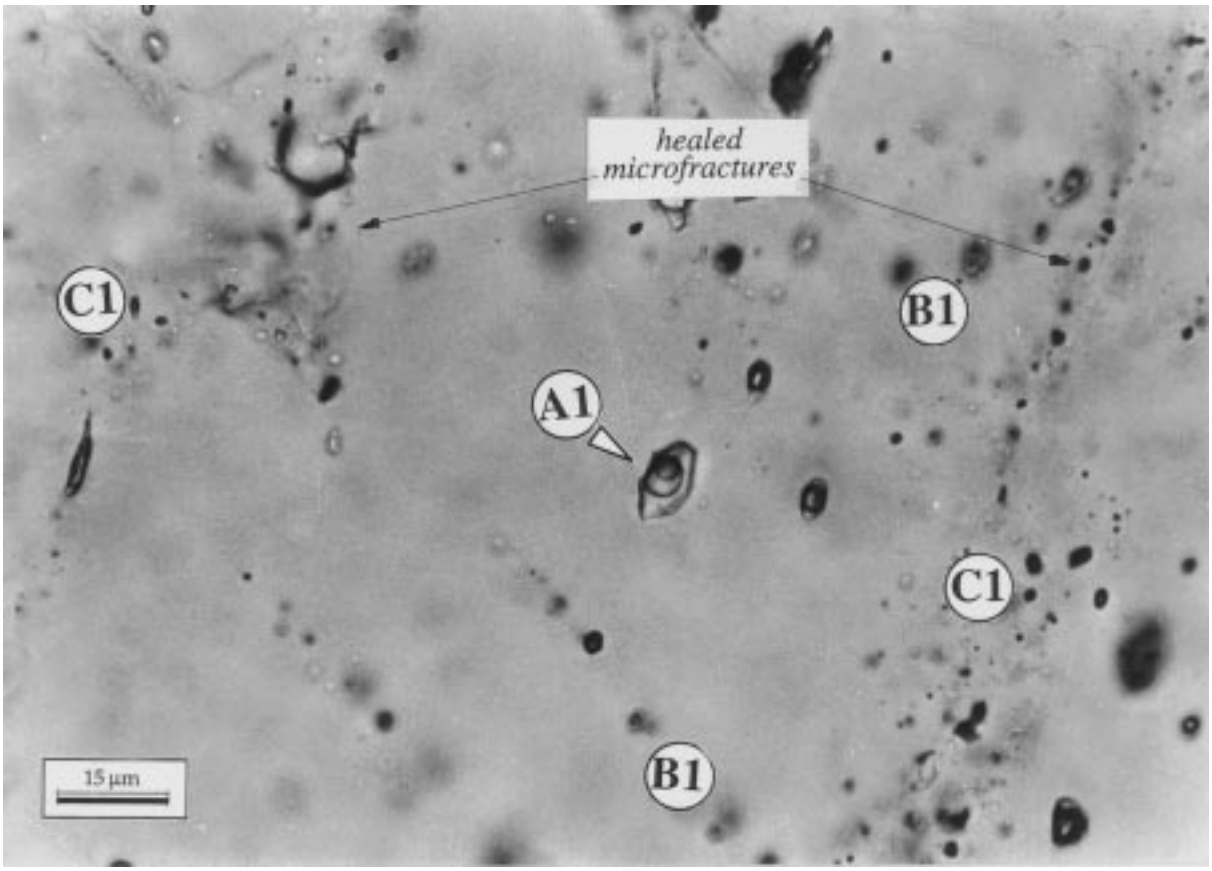

Fig. 9. Photomicrographs showing fluid inclusions in quartz grains from Vein Set 1. A1 is a three-phase (L_{CO_2}, V_{CO_2}, L_{H_2O}) inclusion which occurs typically isolated; mixed CO_2+H_2O type B1 inclusions form short intragranular trails. Type C1 mixed CO_2+H_2O inclusions are present along intergranular healed microfractures.

Type B are CO_2 dominated H_2O–CO_2 inclusions, 5–10 μm in size, with generally negative crystal shapes (Fig. 9). At room temperature, they contain three phases (liquid water, liquid CO_2, and gaseous CO_2) and the CO_2 volume fraction occupies 60–70% of the inclusion volume.

Type C are aqueo-carbonic inclusions, with extremely variable H_2O/CO_2 volume ratios, present along intergranular healed fractures (Fig. 9). Aqueous and CO_2-rich inclusions are observed on separate healed fractures, or are found coexisting along the same trail. Type C inclusions are generally extremely small, < 5 μm in diameter. Rare larger cavities (up to 20 μm) show clear decrepitation features (i.e. star-shaped contours and clusters of small inclusions). Although these inclusions are present in all vein sets, useful measurements were not obtained due to their small size and scarcity.

Fluid inclusion distribution in the different vein sets

Type A inclusions are present in VS1 and VS2 (type A1 and A2, respectively) where they occur as isolated inclusions (Fig. 9) or in small clusters and/or trails in the central part of single quartz grains (Fig. 10). This type of inclusion was not observed within the VS3, lower grade veins. Type A1 and A2 are early (texturally 'oldest') relic inclusions, confined to individual quartz grains, typically found away from subgrain boundaries (Fig. 10). Short intragranular fluid inclusion trails in the VS2 show a strong preferred orientation parallel to the vein wall. The direction of trails is consistent with their development during dynamic growth of quartz, corresponding to primary trapping of fluids.

Type B inclusions are present in all investigated vein sets with different textural features. In VS1 and VS2 veins, respectively, type B1 and B2 aqueo-carbonic inclusions generally occur within quartz grains and along short trails (Fig. 9). In the most deformed samples, where quartz shows deformation lamellae and, in some cases, new subgrain formation, type B1 and B2 inclusions are arranged in short intragranular trails or have a typical polygonal foam distribution, outlining new grain boundaries (Fig. 10). These textural characters indicate that type B1 and B2 inclusions formed during the same event that caused quartz recrystallization in each vein set, after trapping of the respective type A inclusions (Fig. 10).

In VS3, type B3 inclusions are the oldest inclusions observed and occur as isolated individual inclusions or in clusters; they have negative crystal shapes or show

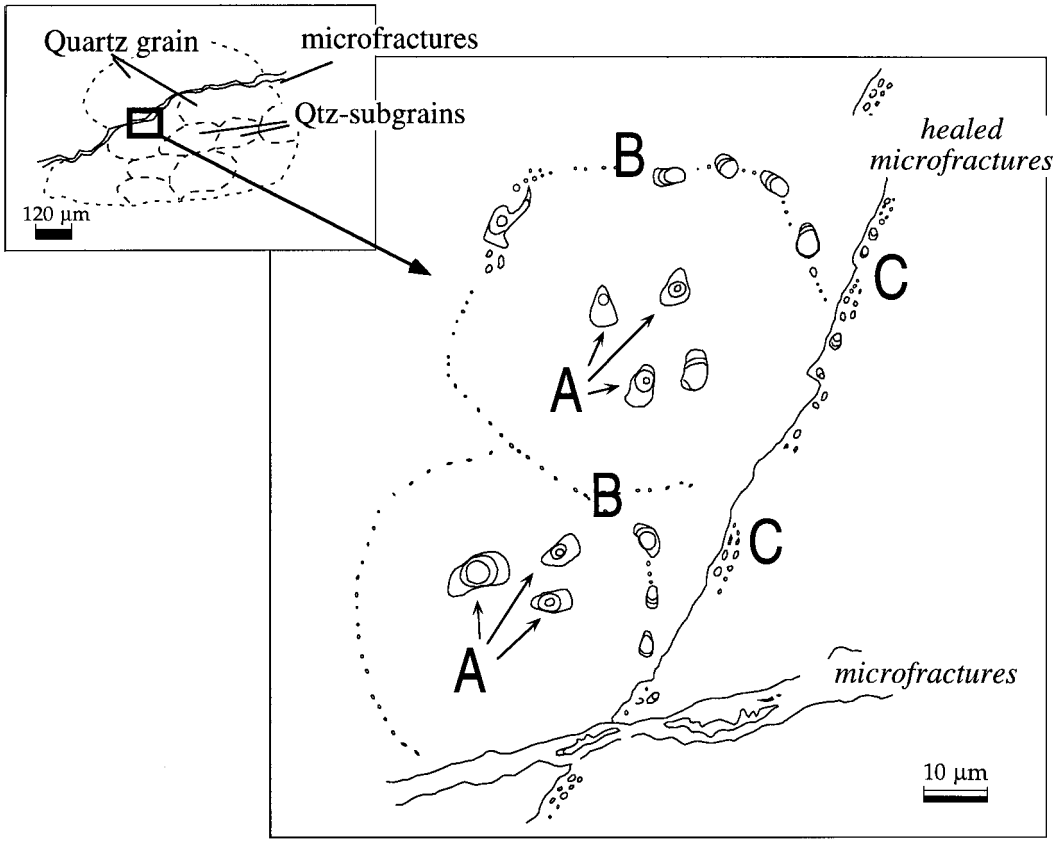

Fig. 10. Schematic representation of microstructural relationships between the various generations of studied fluid inclusions in the different vein sets: Type A: early isolated inclusions present in preserved zones within quartz grains; Type B: late inclusions with typical polygonal distribution lining new sub-grain boundaries; Type C: late trail-bound inclusions present along fractures that cross-cut grain boundaries, see text.

intense re-equilibration features (i.e. star-shaped contours).

Type C inclusions occur along microfractures in all studied vein sets (Fig. 10) with similar late textural characters. The microfractures containing these extremely small inclusions cross-cut quartz grain boundaries and overall features are consistent with fluid trapping as a late tectonic brittle feature during the retrograde exhumation path.

Fluid composition and density

In type A1 and A2 inclusions, temperatures of melting for CO_2 (Tm_{CO_2}) are recorded between −56.9 and −57.7°C (Fig. 11a), below the triple point of pure CO_2 at −56.6°C, indicating that small amounts of low-melting gases are present in the carbonic phase. Raman microspectroscopic analyses indicate that these inclusions contain traces to 4 mol.% $CH_4 \pm N_2$ in the

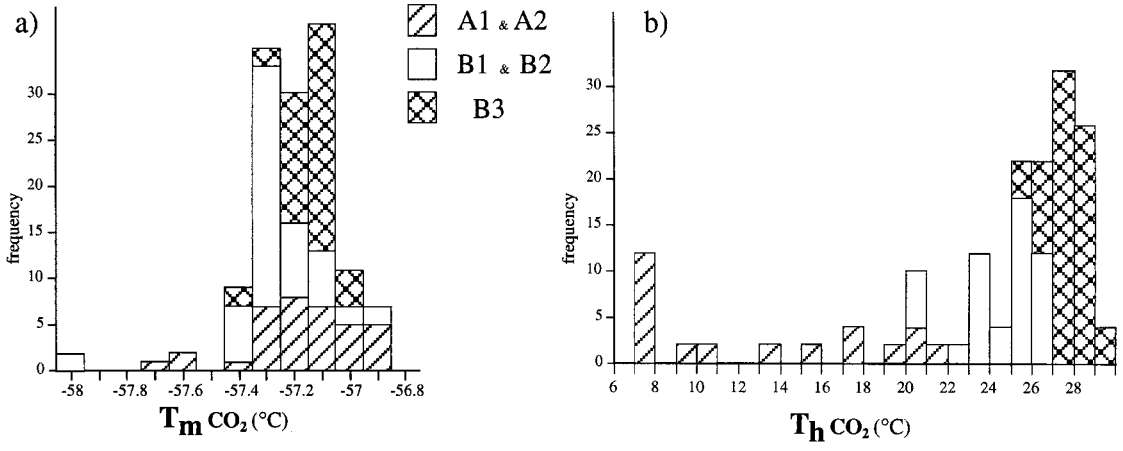

Fig. 11. (a) Histograms of final melting temperature of CO_2 (Tm_{CO_2}) in the three different types of fluid inclusions. (b) Histograms of homogenization temperatures (Th_{CO_2}) of the carbonic phase for fluid inclusions in each vein set.

Table 1. Main characters of representative fluid inclusions. Data collected from fluid inclusions include final melting (Tm) of the CO_2-rich phase and the clathrate phase, and homogenization (Th) of the CO_2-rich phases. See text for further explanations

Inclusion					Carbonic phase					Aqueous phase			Bulk fluid properties				
Type	F vol	Tm °C	Th	L/V	X_{CO_2}	X_{CH_4} mole	X_{N_2}	d g/cm^3	$\bar{V}$ mol/cm^3	Tm clath °C	NaCl wt%	d g/cm^3	X_{H_2O}	X_{CO_2} mol.%	X_{NaCl}	d g/cm^3	$\bar{V}$ mol/cm^3
A1–A2	0.20	−57.4	21.4	*L*	93	4	3	0.76	57.99	7.3	5.15	1.03	0.91	0.07	0.02	0.98	21.00
	0.30	−57.1	17.4	*L*	97	3	0	0.80	54.99	7.0	5.68	1.04	0.86	0.12	0.02	0.97	22.66
	0.20	−57.2	7.9	*L*				0.88	50.18	7.1	5.51	1.04	0.90	0.08	0.02	1.00	20.75
B1–B2	0.50	−56.9	20.9	*L*				0.76	57.57	7.3	5.15	1.03	0.75	0.24	0.01	0.90	27.55
	0.65	−60.0	21.5	*L*		n.d.	n.d.	0.76	58.09	6.9	5.86	1.04	0.61	0.37	0.01	0.85	32.76
	0.55	−57.3	27.4	*L*	98	2	0	0.67	65.73	7.1	5.51	1.03	0.74	0.25	0.01	0.83	30.14
B3	0.50	−57.1	25.8	*L*		n.d.	n.d.	0.70	62.97	7.1	5.51	1.03	0.76	0.22	0.01	0.87	28.15
	0.80	−57.2	26.6	*V*	97	2	1	0.26	166.41	9.1	1.81	1.00	0.69	0.30	0.00	0.41	63.23
	0.65	−57.3	27.9	*V*				0.29	153.41	8.0	3.89	1.02	0.81	0.18	0.01	0.54	42.52

n.d.: not detected. $F = V_{H_2O}/V_{H_2O} + V_{CO_2}$.

CO_2 phase (Table 1). Homogenization temperatures for the carbonic part of the liquid phase (Th_L) lies between 7.5 and 21.4°C (Fig. 11b). Clathrate melting occurs between 4.5°C and 7.3°C and is usually recorded by the sudden movement of the CO_2 gas bubble: these temperatures correspond to a salinity of 5.1–9.7 NaCl eq.wt% in the aqueous part of the fluid.

In the absence of total homogenization temperatures it is possible to calculate composition and densities of the carbonic and aqueous component by combining microthermometry of the carbonic part of the fluid with independent volumetric data (Touret, 1981; Bodnar, 1983). Volumetric proportions of carbonic and water-rich phases in the inclusions ($F = V_{H_2O}/V_{H_2O} + V_{CO_2}$) were estimated optically in regular shaped inclusions using the reference charts from Shepherd *et al.* (1985). The results indicate the same bulk fluid composition for type A1 and A2 inclusions in VS1 and VS2, equal to 86–91 mol.% H_2O, 7–12 mol.% CO_2, NaCl 1.5–2 mol.% NaCl. Bulk densities vary from 0.95 to 1.01 g/cm^3.

In type B1 and B2 inclusions, Tm_{CO_2} ranges between −56.9° and −57.4°C (Fig. 11a), and Th_L for CO_2 is comprised between 20.2 and 27.4°C (Fig. 11b). In a few inclusions, Raman microspectrometry indicates traces to 2 mol.% $CH_4 \pm N_2$. Clathrate melting occurs between 6.6°C and 8°C, corresponding to relative salinities of 3.9–6.4 NaCl eq.wt%. Bulk fluid composition is 13–40 mol.% CO_2, 59–85 mol.% H_2O, and 0.7–1.6 mol.% NaCl, with densities between 0.50 and 0.89 g/cm^3 in both vein sets (Table 1).

In VS3, the isolated early type B inclusions have similar Tm_{CO_2} between −57 and −57.4°C; Raman analyses in selected inclusions indicate that minor CH_4 is present also in this case. At variance with type B1 and B2 inclusions, type B3 inclusions generally homogenize to the vapour phase between 25.2 and 29.2°C (only three inclusions homogenize in the liquid phase at 26°C). Clathrate melting occurs between 7.1 and 9.1°C, corresponding to salinities of 1.8–5.5 NaCl eq.wt%. Bulk fluid composition of type B3 inclusions in VS3 is 59–81 mol.% H_2O, 18–41 mol.% CO_2, 0.5–1 mol.% NaCl (Table 1). The bulk density ranges between 0.43 and 0.87 g/cm^3.

DISCUSSION

Fluid evolution in the decompressive P–T path

A *P–T* path for the formation of the different vein sets in the metasediments of the Voltri massif can be reconstructed comparing the fluid inclusion isochores in the different veins with the *P–T* conditions inferred from mineral compositions in the wall rock.

Distinct fluid inclusion types related to the different veining events should in fact: (1) be texturally the oldest (i.e. for each vein type, the vein forming fluid is considered to be equal to the oldest fluid inclusions), and (2) have isochores that match the inferred *P–T* conditions.

It is inferred from Fig. 8 and from textural characters of fluid inclusions that the earliest circulating fluids (fluid A) are water dominated (H_2O 86–91 mol.%) aqueo-carbonic mixtures, with moderate salinity (5.1–9.7 NaCl eq.wt%) trapped in type A1 and A2 inclusions in VS1 and VS2. In both vein sets, these isolated inclusions are in fact reasonably primary with respect with the veining events, and clearly predate texturally late type B1 and B2 inclusions that line subgrain boundaries or are distributed along healed fractures.

Early type A1 and A2 H_2O–CO_2 fluid inclusions have nearly identical textural characters, composition and density in VS1 and VS2. The type A1 and A2 inclusions, therefore, contain the same fluid phase. The isochores for type A1 and A2 inclusions are similar to each other: for temperatures between 400 and 450°C, the isochores intersect *P* conditions in the range of 6 kbar (Fig. 8a & b) representative of VS1 and VS2 veining during F_1 and F_2 deformation phases.

The flat isochores of type B1, B2 and B3 inclusions imply trapping at much lower pressure (Fig. 8). The isochores for type B1, B2 and B3 inclusions are similar

to each other and in agreement with the late overprint in low greenschist facies, in the mafic rocks, at 2–3 kbar and 350–400°C (Fig. 8a–c). Retrograde metamorphism is associated with influx of aqueo-carbonic mixtures (59–81 mol.% H_2O; fluid B) of low salinity (3.9–6.4 NaCl eq.wt%). Since we have no evidence for immiscibility, minimum temperatures of 330°C at the inferred pressures are provided by the fact that the temperature of trapping should lie above the solvus of the system H_2O–NaCl–CO_2 for this compositions (Fig. 8a–c; Gehrig *et al.*, 1986; Duan *et al.*, 1995).

In early VS1 and VS2 vein sets, retrograde type B fluids are contained in type B1 and B2, which are texturally younger than type A inclusions. Additional evidence for late tectonic origin of B1 and B2 inclusions is their presence in short intragranular trails which indicates that they are contemporaneous to grain-boundary migration.

Present results indicate that the same tectonic event which caused retrogression in VS1 and VS2 also leads to the opening of VS3. Type B fluids, present in the primary type B3 inclusions, are in fact identical to those contained in type B1 and B2 (Table 1).

It is clear from Fig. 8 that the uplift path of the Voltri massif is constrained to transect the lower greenschist conditions determined in the mafic rocks; the resulting path is convex toward the temperature axis and indicates substantial decompression.

Late retrograde fluids in type C inclusions are almost identical in all studied vein sets. In all cases, these are heterogeneous aqueo-carbonic mixtures, probably trapped below the H_2O–CO_2–NaCl solvus (330°C at 2 kbars, Gehrig *et al.*, 1986; Duan *et al.*, 1995). At this stage, quartz recrystallization and the predominant microfracturing indicate that type C fluids were trapped at temperatures compatible with a brittle regime. These fluids were trapped at very late stages, probably at zeolitic facies conditions.

Chemical evolution of the fluid

Present data indicate that the fluid phases which dominated during the retrograde evolution of the Voltri Group were aqueo-carbonic mixtures, where the a_{H_2O} decreased during the glaucophanic and low greenschist's re-equilibration. The chemical similarity between the fluids trapped in type A1 and A2 inclusions related to VS1 and VS2, suggests that the metamorphism and deformation occurred in a closed system.

The data obtained from the *P–T–X* properties of single inclusions related to different metamorphic events have been modelled to calculate f_{O_2} conditions in the fluid inclusions (program FLEVOL in Bakker, 1992). The chemical evolution of fluids is characterized by a progressive decrease of H_2O, and increase of CO_2 (Fig. 12), from the glaucophanic stage (type A fluid) to the low greenschist's re-equilibration (type B fluid). At temperatures of 400–450°C and pressures of 5 kbar, f_{O_2} for early fluids (type A inclusions) is estimated at $10^{-27.3 \pm 0.2}$ MPa, very close to that fixed by the Ni–NiO buffer. An f_{O_2} near to same buffer is obtained also by late fluids (type B inclusions) that yield a value of $10^{-30.6 \pm 0.1}$ MPa at temperatures of 350–400°C and pressures of 2–3 kbar.

This redox trend suggests that the variation in fluid composition at the different retrograde stages probably results from f_{O_2} buffering by rock-forming minerals of enclosing metasediments near the Ni–NiO buffer and suggest an overall closed system fluid-rock evolution during the decompressive *P–T* path. The increase in X_{CO_2} in aqueo-carbonic fluids (Fig. 12), however, is not consistent with regional flow at decreasing *T* at the inferred *P–T–*f_{O_2} conditions. The absence of the expected water enrichment in the fluids calculated for the C–O–H fluid system at the inferred f_{O_2} conditions can have at least two main explanations. (1) Mixed H_2O–CO_2 fluids moving through the metamorphic rocks might have formed hydrous retrograde phases (e.g. muscovite) enriching the residual fluid in CO_2 (trapped as type B inclusions). (2) H_2O may have been lost from the inclusions during re-equilibration processes after trapping. We favour the first hypothesis since the *P–T* conditions of trapping for type B inclusions in VS1, VS2 and VS3 correspond to the estimated conditions of retrograde greenschist re-equilibration.

Significance of fluid inclusion data with respect to folding events

Physico-chemical conditions reconstructed for early type A and B fluids are evidence for fluid trapping during a complex succession of veining events, which characterizes the retrograde metamorphic evolution in

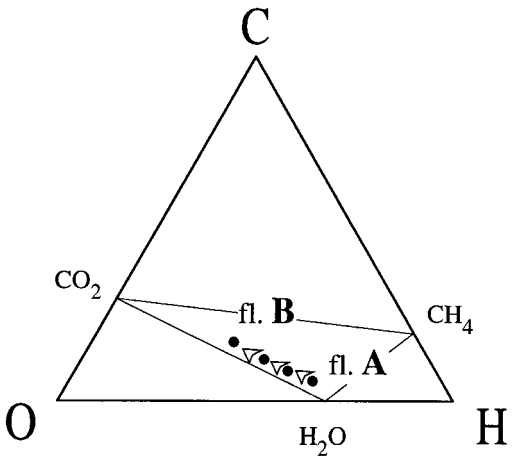

Fig. 12. C–O–H diagram showing evolution of the fluid composition (mole fraction) during decompression and cooling. The chemical evolution of fluids is characterized by a progressive decrease of H_2O, and increase of CO_2 from the glaucophanic to the low greenschist facies re-equilibration. Filled circles: calculated compositions for type A and type B fluids in mol.%.

the Voltri metasedimentary rocks. The reconnaissance of identical P–T–X characters in A1 and A2 fluid inclusions (type A fluids) associated, respectively, with F_1 and F_2 events allows at least two different interpretations:

1. A1 fluid inclusions are representative of original trapping P–T conditions at 450° and 6 kbars: VS1 reflect the last stages of F_1 folding during a progressive and continuous deformational event from F_1 to F_2 conditions. If this is the case, the P conditions of VS1 veining are not coincident with the P conditions of phengite growth.
2. A1 fluid inclusions are contemporaneous with VS1–F_1 at 7–8 kbar as indicated by Velde's geobarometer, but original densities have been re-equilibrated during the VS2–F_2 formation at lower pressure (≈6 kbar): the composition of the fluids circulating through rocks may have been similar during F_1 and F_2 (i.e. metamorphism and deformation occurred in a closed system), but the P–V properties of these fluids were originally different.

The possibility that densities of early fluid inclusions in VS1 were reset during the F_2 folding event cannot be excluded *a priori*. The P–T–t path determined for the basic rocks is very steep (Fig. 2) and might have induced overpressure allowing slow re-equilibration during the retrograde metamorphic evolution. However, if all inclusions had re-equilibrated in response to decreasing P (decrepitation processes; $P_{\text{fluid inclusions}} \gg P_{\text{external}}$) a rather large range of resulting densities should have been expected. Indeed as re-equilibration of fluid inclusions with respect to density must depend on many factors (i.e. composition and size), the final re-equilibration conditions should have been different for each inclusion. The observed microstructural features indicate that decrepitated type A1 inclusions are only a minority—which was not analysed—and fluid composition is rather constant ($X_{CO_2} \approx 0.1$). The range in P–T values for A1 inclusion isochores is tighter than the one defined by A2 inclusions (cf. Fig. 8a & b), suggesting that re-equilibration processes, if present, were of little importance. In addition, the retrograde metamorphic gradient is similar to the steep isochore trends, so that the inclusions may have maintained similar densities during decompression ("safety channelways" of Touret, 1992).

Independent evidence for a progressive and continuous deformation from F_1 to F_2 folding in the metasediments has been revealed by structural analysis (Crispini and Capponi, 1997), and by the fact that the development of the F_1 and F_2 folds occurred under very similar P–T conditions during the glaucophanic and/or barroisitic stage (Fig. 13).

Based on these arguments, the first interpretation seems to be the most likely for the interpretation of the similarities between circulating fluids (types A1 and A2 fluid inclusions) during F_1 and F_2 folding episodes. Present results support the hypothesis that F_1 and F_2 shear folds do not result from two distinct folding episodes, but reflect a single progressive deformational event that covers a definite range in the P–T–t space.

F_3 folds developed at a later stage, probably corresponding to the lower greenschist facies re-equilibration (3 kbar and 400°C; Fig. 13). At these stages, quartz in vein sets 1 and 2 underwent grain boundary migration and subgrain formation, as witnessed by the typical honeycomb distribution of type B inclusions in both sets of veins. The bulk chemical composition indicates that late fluids are enriched in CO_2 with respect to early fluids. The decrease in water content (from 90 mol.% to 60–70 mol.%) in the fluids can be due to the ongoing water-consuming hydration reactions, which are expected to have taken place during retrograde P–T conditions.

CONCLUSIONS

The study of fluid evolution in veins associated to folding events provides an independent and complementary investigation tool to examine the relationships between different folding events. As geometrical features alone cannot be used with confidence as correlation criteria (Williams, 1985), this case study indicates that fluid inclusion analysis applied to structural investigations can provide constraints on the overall fluid evolution and, as a consequence, on the relative timing of related deformations.

In the Voltri Group, combined fluid inclusion, meso- and microstructural data outline that no significant change in the physical–chemical conditions occurred in the conditions of fluid trapping during the development of F_1 and F_2 folds: there is no change in the fluid composition, which probably indicates that the same aqueo-carbonic fluid (20 mol.% CO_2) is trapped at early stages in the two vein sets; and there is no significant variation in the P and T of trapping. The results of this study match the structural evidence that F_1 and F_2 folds formed in a single progressive and

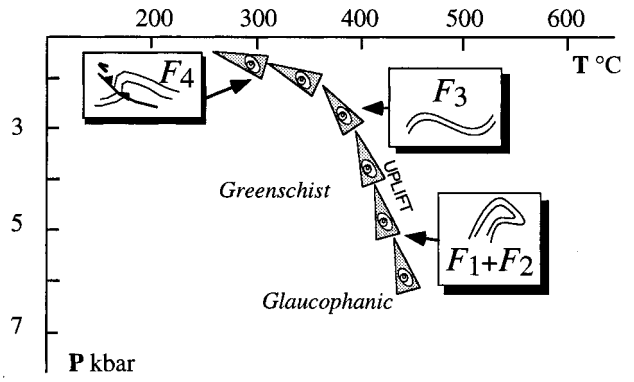

Fig. 13. Summary of the P–T–t evolution inferred from the analysis of fluids in Vein Set 1–2–3. Related folding structures are indicated.

continuous deformational event, starting from the glaucophanic and/or barroisitic stage, during the uplift phase of the tectonic evolution.

On the other hand the fluids related to the formation of F_3 folds are significantly different. The chemical composition of the trapped fluids changes in more CO_2-rich aqueo-carbonic mixtures and trapping occurred at shallow levels, at the P–T conditions of the low greenschist overprints (3 kbar and 400°C). Despite the style of the folds, fluid composition indicates that F_3 structures formed at different P–T conditions than other phases.

Acknowledgements—Funding for this research was provided by the EC Human Capital and mobility "hydrothermal: metamorphic water-rock interaction in crystalline rocks: a multidisciplinary approach on paleofluid analysis" and by Italian M.U.R.S.T. (Ministero per l'Università e per la Ricerca Scientifica e Tecnologica). The authors are indebted to M. Cathelineau, M. C. Boiron and J. Dubessy for useful discussions and hospitality to L.C. at the C.R.E.G.U. in Nancy. RAMAN analyses were performed by B. C. Boiron and L.C. at the C.R.E.G.U. in Nancy. The paper has been improved by critical and helpful comments by A. M. Bouiller, R. J. Bakker and J. L. R. Touret. We thank G. Capponi and G. Giorgetti for helpful discussions on an earlier version of the manuscript.

REFERENCES

Bakker, R. J. (1992) On modifications of fluid inclusions in quartz, re-equilibration experiments and thermodynamical calculations on fluids in natural quartz. PhD Thesis, Geologica Ultraiectina.

Bakker, R. J. (1995) The application of a computerized and optimized clathrate stability model to fluid inclusion studies. *Boletín de la Sociedad Española de Mineralogía* **18,** 15–17.

Bakker, R. J. and Jansen, J. B. H. (1990) Preferential water leakage from fluid inclusions by means of mobile dislocations. *Nature* **345,** 58–60.

Bakker, R. J. and Jansen, J. B. H. (1991) Experimental post-entrapment water loss from synthetic CO_2–H_2O inclusions in natural quartz. *Geochimica et Cosmochimica Acta* **55,** 2215–2230.

Bakker, R. J. and Jansen, J. B. H. (1994) A mechanism for preferential H_2O leakage from fluid inclusions in quartz, based on TEM observations. *Contributions to Mineralogy and Petrology* **116,** 7–20.

Bakker, R. J. (1997) Clathrates: computer programs to calculate fluid inclusion V–X properties using clathrate melting temperatures. *Computers and Geosciences* **23,** 1–18.

Bodnar, R. J. (1983) A method of calculating fluid inclusion volumes based on vapor bubble diameters and P–V–T–X properties of inclusion fluids. *Economic Geology* **78,** 535–542.

Bodnar, R. J., Binns, P. R. and Hall, D. N. (1989) Synthetic fluid inclusions—VI. Quantitative evaluation of the decrepitation behaviour of fluid inclusions in quartz at one atmosphere confining pressure. *Journal of Metamorphic Geology* **7,** 229–242.

Boullier, A. M., France-Lanord, C., Dubessy, J. and Champenois, M. (1991) Linked fluid and tectonic evolution in the High Himalaya mountains (Nepal). *Contributions to Mineralogy and Petrology* **107,** 358–372.

Bowers, T. S. and Helgeson, H. C. (1983) Calculation of the thermodynamic and geochemical consequences of nonideal mixing in the system H_2O–CO_2–NaCl on phase relations in geological systems: metamorphic equilibria at high pressure and temperatures. *American Mineralogist* **68,** 1059–1075.

Brown, P. E. and Hagemann, S. G. (1994) MacFlincor: a computer program for fluid inclusion data reduction and manipulation. In *Fluid inclusions in minerals: methods and applications*, eds B. De Vivo and M. L. Frezzotti, pp. 231–250. Virginia Tech, Blacksburgh.

Brown, P. E. and Lamb, W. M. (1989) P–V–T properties of fluids in the system $H_2O \pm CO_2 \pm$NaCl: new graphical representation and implications for fluid inclusion studies. *Geochimica et Cosmochimica Acta* **53,** 1209–1221.

Burkhard, N. (1993) Calcite twins, their geometry appearance and significance and stress–strain markers indicators of tectonic regime: review. *Journal of Structural Geology* **15,** 351–368.

Cabella, R., Cortesogno, L., Gaggero, L. and Lucchetti, G. (1994) Clinopyroxenes through the blueschist facies metamorphism of the Liguria Alps: compositional variability and miscibility gaps. *Atti Ticinesi di Scienze della Terra, Ser. Spec.* **1,** 55–63.

Capponi, G. (1991) Megastructure of the South-Eastern part of the Voltri Group (Ligurian Alps): a tentative interpretation. *Bollettino della Società Geologica Italiana* **110,** 391–403.

Chiesa, S., Cortesogno, L., Forcella, F., Galli, M., Messiga, B., Pasquarè, G., Pedemonte, G. M., Piccardo, G. B. and Rossi, P. M. (1975) Assetto strutturale ed interpretazione geodinamica del Gruppo di Voltri. *Bollettino della Società Geologica Italiana* **94,** 555–582.

Cimmino, F. and Messiga, B. (1979) I calcescisti del Gruppo di Voltri (Liguria Occidentale): le variazioni composizionali delle miche bianche in rapporto alla evoluzione tettonico-metamorfica Alpina. *Ofioliti* **4,** 269–294.

Cortesogno, L., Ernst, W. G., Galli, M., Messiga, B., Pedemonte, G. M. and Piccardo, G. B. (1977) Chemical petrology of eclogitic lenses in Serpentinite, Gruppo di Voltri, Ligurian Alps. *Journal of Geology* **85,** 255–277.

Crispini, L. (1996) Evoluzione Strutturale dei Metasedimenti del Gruppo di Voltri e della Zona Sestri-Voltaggio: implicazioni nell'evoluzione Tettonica e Geodinamica Alpina. PhD Thesis. ERSU, Università di Genova.

Crispini, L. and Capponi, G. (1997) Quartz fabric and strain partitioning in sheath folds: an example from the Voltri Group (Ligurian Alps, Italy). *Journal of Structural Geology* **19,** 1149–1157.

de Vivo, B. and Frezzotti, M. L. (1994) *Fluid inclusions in minerals: methods and applications*. Virginia Tech, Blacksburgh.

Duan, Z., Moller, N. and Weare, J. H. (1995) Equation of state for the NaCl–H_2O–CO_2 system: Prediction of phase equilibria and volumetric properties. *Geochimica et Cosmochimica Acta* **59,** 2869–2882.

Gehrig, M. (1980) Phasengleiche und P–V daten ternarer Mischungen aus Wasser, Kohlendioxid und Naturiumchlid bis 3 kbar und 550°C. PhD Thesis. University of Karlsruhe.

Gehrig, M., Lentz, H. and Franck, E. U. (1979) Thermodynamic properties of water carbon-dioxide–sodium-chloride mixtures at high temperatures and pressures. In *Pressure Science and Technology*. *Physical Properties and Material Synthesis*. pp. 539–542. Plenum Press, New York.

Gehrig, M., Lentz, H. and Franck, E. U. (1986) The system water–carbon dioxide–sodium chloride to 773 K and 300 MPa. *Berichte der Bunsengesellschaft Physikalische Chemie* **90,** 525–533.

Hanmer, S. and Passchier, C. W. (1991) Shear-sense indicator: a review. *Geological Survey of Canada* **90,** 1–72.

Hodgkins, M. A. and Stewart, K. G. (1994) The use of fluid inclusions to constrain fault zone pressure, temperature and kinematic history: an example from the Alpi Apuane, Italy. *Journal of Structural Geology* **16,** 85–96.

Hollister, L. S. and Crawford, M. L. (1981) Short course in fluid inclusions: applications to petrology. *Mineralogical Association of Canada* **6,** 304 pp.

Hoogerduijn Strating, E. H. (1991) The evolution of the Piemonte–Ligurian ocean. A structural study of ophiolite complexes in Liguria (NW Italy). *Geologica Ultratraiectina* **74,** 1–145.

Massonne, H.-J. and Schreyer, W. (1987) Phengite Geobarometry based on the limiting assemblage K-feldspar, phlogopite and quartz. *Contributions to Mineralogy and Petrology* **96,** 212–224.

Messiga, B. and Scambelluri, M. (1991) Retrograde P–T–t path for the Voltri Massif eclogites (Ligurian Alps, Italy): some tectonic implications. *Journal of Metamorphic Geology* **9,** 93–109.

Messiga, B., Scambelluri, M. and Piccardo, G. B. (1995) Chloritoid-bearing assemblages in mafic systems and eclogite-facies hydration of alpine Mg–Al metagabbros (Erro-Tobbio Unit, Ligurian Western Alps). *European Journal of Mineralogy* **7,** 1149–1167.

Mullis, J. (1996) P–T–t path of quartz formation in extensional veins of the Central Alps. *Schweiterische Mineralogische und Petrographische Mitteilungen* **76,** 159–164.

Platt, J. P. and Vissers, R. L. M. (1980) Extensional structures in anisotropic rocks. *Journal of Structural Geology* **2,** 397–410.

Poty, B., Leroy, J. and Jachimowicz, L. (1976) Un nouvelle appareil pour la mesure des temperaturés sous le microscope: l'installation de microthermométrie Chaixmeca. *Bulletin of Mineralogy* **99,** 182–186.

Ramsay, J. G. and Huber, M. I. (1987) *The techniques of modern structural Geology*. *Volume 2: folds and fractures*. Academic Press, London.

Roedder, E. (1984) Fluid inclusions. *Reviews in Mineralogy* **12,** 1–644.

Shepherd, T., Rankin, A. H. and Alderton, D. H. M. (1985) *A practical guide to fluid inclusions studies*. Blackie, Glasgow.

Sterner, S. M. and Bodnar, R. J. (1989) Synthetic fluid inclusions—VII. Re-equilibration. Quantitative evaluation of the decrepitation behaviour of fluid inclusions in quartz. *Journal of Metamorphic Geology* **7,** 243–260.

Sterner, S. M., Hall, D. L. and Keppler, H. (1995) Compositional re-equilibration of fluid inclusions in quartz. *Contributions to Mineralogy and Petrology* **119,** 1–15.

Touret, J. L. R. (1981) Fluid inclusions in high-grade metamorphic rocks. In *Short Course in Fluid Inclusions: Application to Petrology*. pp. 182–208, eds L. S. Hollister and M. L. Crawford. Mineralogical Association of Canada, **6**.

Touret, J. L. R. (1987) Fluid inclusions and temperature–pressure estimates in deep-seated rocks. In *Chemical transport in metasomatic processes*, ed. H. C. Helgeson, pp. 1–781. NATO ASI C218, Reidel Publication.

Touret, J. L. R. (1992) CO_2 transfer between the upper mantle and the atmosphere: temporary storage in the lower continental crust. *Terra Nova* **4,** 87–98.

Velde, B. (1967) Si^{4+} content of natural Phengite. *Contributions to Mineralogy and Petrology* **14,** 250–258.

Vityk, M. O. and Bodnar, R. J. (1995a) Do fluid inclusions in high-grade metamorphic terranes preserve peak metamorphic density during retrograde decompression? *American Mineralogist* **80,** 641–644.

Vityk, M. O. and Bodnar, R. J. (1995b) Textural evolution of synthetic fluid inclusions in quartz during reequilibration, with applications to tectonic reconstruction. *Contributions to Mineralogy and Petrology* **121,** 309–323.

Werling, E. (1992) Tonale-, Pejo- und Judiacien-linie: kinematik, mikrostrukturen und metamorphose von tektoniten aus raumlich interferierenden aber verschiedenaltrijen verwerfungszonen. PhD Dissert. E.T.H., Zurigo.

Williams, P. (1985) Multiply deformed terrains—problems of correlation. *Journal of Structural Geology* **27,** 269–280.

Zhang, Y. G. and Frantz, J. D. (1987) Determination of the homogenization temperatures and densities of supercritical fluids in the system NaCl–KCl–$CaCl_2$–H_2O using synthetic fluid inclusions. *Chemical Geology* **64,** 335–350.